ORIGINAL ARTICLE

Effects of cold rolling and annealing on the ridging behaviour of ferritic stainless steel

Xiaoguang Ma [1] · Jingwei Zhao [1] · Wei Du [2] · Zhengyi Jiang [1]

Abstract

A systematic study was carried out to evaluate the effects of cold rolling and annealing processes on the ridging severity of ferritic stainless steel (FSS). Both microstructural refinement and texture optimisation were achieved with an optimised processing schedule to improve the ridging resistance of FSS. Coarse grain bands comprising of primarily {112} <110> oriented grains were found to form inside cold-rolled and annealed FSS sheets. The effects of annealing schedules and the resultant microstructure and texture on the ridging behaviour of FSS are discussed. The results indicate that the reduction in the fraction of {001} <110> orientation by optimisation of the rolling processes contributes to reduce the ridging height of the FSS during the subsequent forming process. Through extending soaking time and under 880 °C during final annealing step, a maximum of 30% reduction in ridging height can be achieved with a refined microstructure and texture of FSS, improving the surface quality of FSS during subsequent forming processes.

1 Introduction

With a growing demand of new materials with low cost and good mechanical properties, development of steel grades with good mechanical and functional performance is becoming increasingly important in manufacturing engineering. Such considerations promote the development and application of ferritic stainless steels in a variety of fields, such as automobiles engineering, medical science and electronic engineering [1, 2]. With its good corrosion resistance, high thermal conductivity and low cost during manufacturing processes, FSS 430 is widely used for various applications such as kitchenware, automotive exhaust systems and elevator panels [3, 4].

However, the occurrence of ridging during the forming process can significantly hamper the surface quality of the FSS. Ridging is an undesirable surface corrugation with a depth varying from 10 to 50 μm that arises during stretching or deep drawing. Severe surface ridging may deteriorate the surface appearance of the formed products of FSS, which requires further polishing operations and increases the operation cost during manufacturing process. Suppression of the ridging phenomenon, therefore, has been investigated by researchers in order to improve the surface quality of the resultant products and reduce the operation cost during subsequent forming processes. Although segregation of the alloying elements (C, Cr and Mo) affects the formation of ridging, it is commonly acknowledged that ridging is generated due to the different anisotropic plastic deformation of neighbouring grains with different crystallographic textures [5, 6].

The role of crystallographic texture on the ridging severity of FSS has been widely reported by researchers. Defilippi and Chao [1] stated that ridging is generated due to the different plastic strain ratios between the ND // <111> and ND // <100> components. A crystal plasticity (CP) model was proposed by Takechi et al. [2] to investigate the correlation between texture and ridging, and the results indicate that ridging can be attributed to the different shear strains between RD // <110> fibres. The correlation of microstructure and ridging was also

✉ Zhengyi Jiang
   jiang@uow.edu.au

   Xiaoguang Ma
   xm966@uowmail.edu.au

   Jingwei Zhao
   jwzhaocn@gmail.com

1 School of Mechanical, Materials and Mechatronic Engineering, University of Wollongong, Wollongong, NSW 2522, Australia

2 Stainless Steel Technical Centre, Baosteel Research Institute (R&D Centre), Baoshan Iron & Steel Co., Ltd., Shanghai 200431, China

investigated by Engler et al. [3] using both numerical simulation and experimental methods. The authors stated that the occurrence of ridging is caused by the collective deformation of band-like clusters of grains with similar crystallographic orientations. Kuntsen and Wittridge [4] studied parallel surface ridging in FSS during uniaxial tensile straining, and found that the corrugation profile was related to the superimposition of a number of differential transverse strains. Huh et al. [5] analysed the effect of through-thickness macro- and micro-texture gradients on ridging of 17% Cr FSS sheet and found that the elongated orientation colonies that formed close to the sheet centre were responsible for ridging in the cold-rolled and recrystallised FSS sheet. To further investigate the texture-induced surface ridging, EBSD tests were conducted by Bennett et al. [6] to characterise the microstructure of specimens before and after tensile stretching. The results indicate that the cube bands promote ridging generation on the surface of automotive aluminium sheet during the forming process. The development of the ridging phenomenon in automotive aluminium sheets was also studied by Baczynski et al. [7] using X-ray diffraction (XRD) tests. The authors stated that the spatial distribution of the Goss component is responsible for directional roughening and ridging generation after tensile stretching.

Given that texture is commonly considered to be responsible for ridging generation, the optimisation of rolling parameters has been investigated by a number of researchers to obtain optimal texture components and improve the surface quality of polycrystalline materials during the subsequent forming processes. The influence of hot band annealing and cold rolling on the texture and ridging of FSS 430 was analysed by Patra and Singhal [8]; it was found that hot-rolled coils annealed by slow cooling under insulated cover exhibit better ridging resistance than bell annealing treatment. In addition, the direct effect of coarse grain streaking on the formation of ridging in FSS was demonstrated by Patra et al. [9] using EBSD tests. A sufficiently high temperature during hot band annealing was recommended by the authors in order to refine the coarse, cube-oriented grains by recrystallisation. The effects of hot-rolled shear bands on the surface ridging of FSS were analysed by Zhang et al. [10], and the results indicate that the existence of shear bands can enhance the nucleation for recrystallisation during hot rolling and annealing for microstructural refinement. The effects of cold rolling processes on microstructure and texture were discussed by Gao et al. [11]; it was found that ridging could be significantly alleviated with a proposed two-step cold rolling process. The development of γ-fibre recrystallisation texture was found to be responsible for ridging generation of FSS during forming processes. The correlation between heat treatment and ridging phenomenon of FSSs was analysed by Park and Park [12]. The results indicate that the ridging phenomena are dramatically improved with annealing temperatures higher than

920 °C due to the recrystallisation of the band structure. The effects of processing optimisation on ridging development of FSS were demonstrated by Han et al. [13] by means of optical microscopy, XRD and EBSD tests. The authors stated that the addition of a warm-rolling procedure leads to refinement of grain size and modification of texture, inducing a remarkable improvement in the anti-ridging performance of FSS during the subsequent forming processes. Mola et al. [14] evaluated the effects of thermomechanical processing on the ridging resistance of FSS 430 and found that the presence of the γ-phase benefits the ridging resistance of this alloy. Dorner et al. [15] analysed the retention of the Goss component between microbands during cold rolling and found that the Goss-oriented bands aligned in shear bands formed during straining, giving a rise to ridging generation of FSS. The formation mechanisms of the cube recrystallisation texture in cold-rolled steel were studied by Zaefferer et al. [16] by means of X-ray texture measurement and transmission electron microscopy. It was stated that the misorientation across the orientation gradient in the cube bands increases with increasing deformation. Given that the texture is affected by the formation process, it is significant to investigate the correlation between texture and processing routes.

Although the effects of thermomechanical processing on the ridging resistance of FSS have been discussed by researchers, few published works have focused on the correlation between annealing time, temperature and ridging severity of FSS 430 during the subsequent forming processes. In this study, a series of experiments were conducted in order to analyse the microstructure and texture evolution during rolling and annealing with different routes. The relationship between the annealing temperature and soaking time on texture-induced ridging is investigated to obtain optimal parameters to alleviate the ridging phenomenon of FSS 430. This work aims to develop effective strategies in rolling routes for improving the ridging resistance of FSS 430 through investigation into the relationship between the annealing temperatures, soaking time, microstructure, texture and ridging resistance of FSS 430.

1.1 Materials and experimental procedures

An industrial FSS 430 was utilised for the present study. The chemical composition of the FSS 430 is given in Table 1. Detailed schematic diagrams are illustrated in Table 2. Cast slabs of 5-mm thickness were hot-rolled to 1 mm using

Table 1 Chemical composition (wt%) of FSS 430

Material	C	Si	Mn	S	P	Cr	N
FSS 430	0.049	0.35	0.23	0.002	0.031	16.24	0.0348

Table 2 Diagrams of the processing schedule

Rolling schedule	A	B	C	D
Hot rolling pass 1 (35% reduction)	1150 °C	1150 °C	1150 °C	1150 °C
Hot rolling pass 2 (35% reduction)	1050 °C	1050 °C	1050 °C	1050 °C
Hot rolling pass 3 (35% reduction)	950 °C	950 °C	950 °C	950 °C
Hot rolling pass 4 (30% reduction)	850 °C	850 °C	850 °C	850 °C
Intermediate annealing	840 °C, 2 h	840 °C, 2 h	840 °C, 2 h	840 °C, 2 h
Cold rolling (70% reduction in 4 passes)	25 °C	25 °C	25 °C	25 °C
Final annealing	850 °C, 1 min	850 °C, 3 min	880 °C, 1 min	880 °C, 3 min

tandem rolling in 4 passes with the temperature decreasing from 1150 to 850 °C, and then air cooled down to room temperature. After annealing at 840 °C for 2 h, the specimens were cold-rolled with multiple passes using a four-high rolling mill followed by subsequent annealing. With different schedules of annealing processes, the effects of the cold rolling and annealing processes on the microstructure, texture and ridging resistance of FSS 430 can be analysed. The rolling experiments in the present study were conducted on a Hille-100 experimental rolling mill. The rolls are made of high-speed steels with a length of 254 mm and a diameter of 225 mm. The rolling speed of rolls is set to 0.6 m/s in the present study. The rolling mill is driven by a 56-kW hydraulic system with a maximum rotating speed of 60 rpm, whilst the maximum load and torque can reach up to 1000 kN and 12.7 kN·m, respectively. The details of the final annealing followed in each schedule are summarised below.

The cross-sections of the cold-rolled and annealed specimens were electro-polished for microstructure characterisation and texture study. A solution of 90% methanol and 10% perchloric acid was utilised for electro-polishing in the present study. The EBSD tests were performed with a step size of 2 μm using an Oxford HKL Channel 5 system. To ensure a high accuracy of EBSD mapping, noise reduction was performed by giving the most common neighbouring orientation to each zero solution point. The distribution of crystallographic orientations was represented in the form of orientation distribution functions (ODFs) of the $\varphi 2 = 45°$ section of the Euler space. The grain size distributions of cold-rolled and annealed specimens were evaluated by measuring the grain area and equivalent circle diameter grain size of grains, following the techniques proposed by Patra et al. [9].

A series of tensile tests were conducted to investigate the ridging phenomenon of FSS 430. The specimens were prepared following the ASTM E8-E8M Standard [17] (as shown in Fig. 1) and were tested using an Instron 5566 test system at room temperature. All tests were carried out with 20% extension with the speed of 1 mm/min. The tests were conducted three times under each condition and the average value of ridging height was utilised to evaluate the ridging resistance

of FSS 430. The obtained stress-strain curve of FSS 430 is displayed in Fig. 2 and the diagram of the whole process is illustrated in Fig. 3.

2 Results and discussion

2.1 Microstructure characterisation

The microstructures of cold-rolled and annealed specimens under different annealing schedules are shown in Fig. 4. The measured region is the cross-section of the FSS sheet after tensile deformation, as shown in Fig. 5. Undulations are also a function of texture and microstructure but on a larger scale. In this case, it is the anisotropic plastic behaviour of larger volumes involving several {111} <uvw> and {001} <uvw> colonies that should be looked at.

The IPF maps of the cold-rolled and annealed FSS sheet are shown in Fig. 4. It can be seen that refined grains are formed at surface layers after rolling processes. It is known that the surface layers are subjected to profound driving force during rolling, and significant shear deformation on the grains in the surface layers was caused [18]. The grains on the surface layers, therefore, are refined during recrystallisation. The grains in the central layers, on the other hand, are mainly subjected to plane-strain compression which cannot refine the grains' effectively unlike the grains in the surface layers. The grain colonies, therefore, remain at central layers of the FSS sheet during rolling processes. The formation of grain colonies promotes the inhomogeneity of grain sizes and significantly affects the anisotropy of FSS 430. As shown in Fig. 4, the microstructure of specimens after final annealing was characterised by equiaxed grains and pancake-shaped grains originating from static recovery during annealing. With higher annealing temperature and soaking time, a remarkable reduction in elongated grains can be observed during recrystallisation.

For specimens annealed under schedule D, the cold-rolled sheet was fully recrystallised and the microstructure comprised by equiaxed grains, as shown in Fig. 4(d). The average
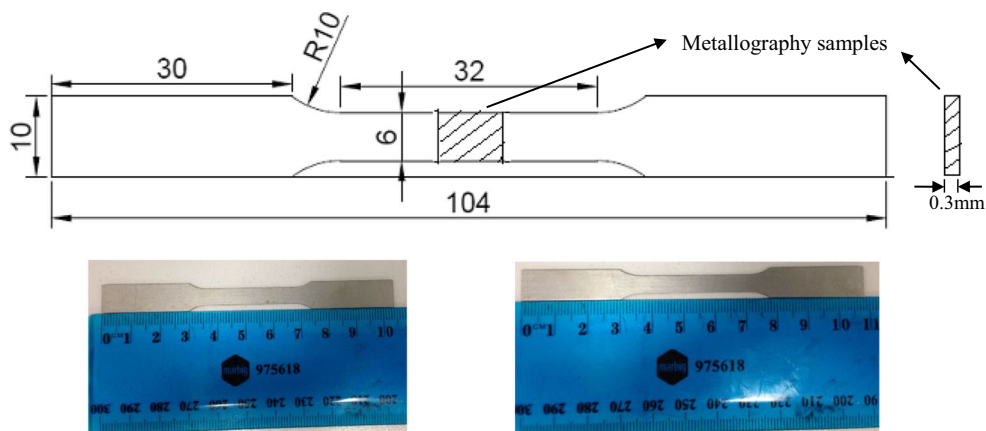
grain sizes in the final sheets are given in Fig. 5. With the increase of annealing temperature and soaking time, the residual non-recrystallised region continued to recrystallise and more refined grains formed in specimen, giving a rise to the growth of the average grain size of the annealed FSS sheet. Meanwhile, the residual deformed grains were replaced by recrystallised, equiaxed grains during the annealing process.

2.2 Texture evolution

The ODF sections of FSS sheets processed under different rolling schedules are given in Fig. 6. For a quantitative analysis of the textures, ODFs $f(g)$ were calculated from the EBSD data by associating each orientation $g = \{\varphi 1, \Phi, \varphi 2\}$ with a narrow Gauss-shaped peak with a (half) scatter width $\psi_0 = 2°$ in Euler space [19]. The resulting ODFs presented in Fig. 6 are in the form of iso-intensity lines in three characteristic sections through the Euler angle space. With this representation, orthotropic sample symmetry is implicitly assumed, as given by the orthogonal sample axes RD and ND.
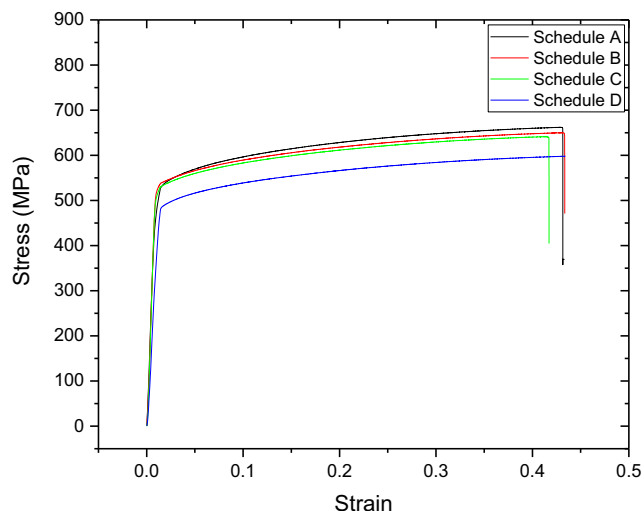
Fig. 2 Stress-strain curves of FSS 430 under different rolling routes

As shown in Fig. 6, the annealed specimens show the typical hot band texture of FSS which is characterised by prominent texture consisting of the α-fibre with a maximum close to the {001} <110> and {115} <110> orientations. The specimens annealed at 850 °C for 1 min show the dominance of the {001} <110> orientation, which is considered to be one of the major components leading to ridging generation of FSS [20]. The intensity of the {115} <110> component was a minimum in the specimen processed under schedule D, Fig. 6. FSS 430 undergoes rapid dynamic recovery preceding recrystallisation during hot rolling, which restricts texture randomisation through dynamic recrystallisation and phase transformation [21]. The strong {115} <110> component, therefore, can be developed from columnar grains with the {001} <110> component. The {001} <110> component can transform into the {111} <112> orientation after recrystallisation, although the transformation rate is slow due to the low stored energy of the {001} <110> component.
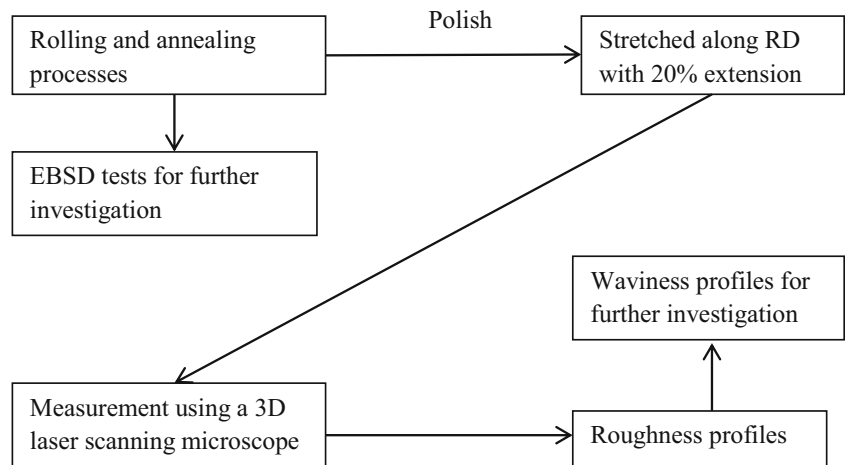
For specimens annealed under schedules A, B and C, weak orientations scattering along the γ-fibre were observed due to incomplete recrystallisation. With the increase of annealing temperature and holding time, the texture components along the γ-fibre gradually formed as shown in Fig. 6. During the annealing process after cold rolling, a typical γ-fibre recrystallisation texture was formed under schedule D with strong intensity at the {334} <483> and {111} <112> components.

2.3 Evolution of the grain boundary

After rolling and subsequent annealing processes, the initial grain boundaries have been broken into mixed grain boundary structures composed of low-angle boundaries (LABs), elongated high-angle boundaries (HABs) and equiaxed new HABs formed during recrystallisation. Figure 7 shows the distribution of the misorientation angle and coincidence site lattice (CSL) boundary of FSS 430 annealed under different schedules. The misorientation angle distributions indicate that

Fig. 3 Diagrams of processes

```
┌─────────────────────┐        Polish        ┌─────────────────────┐
│ Rolling and annealing│────────────────────▶│ Stretched along RD  │
│ processes            │                      │ with 20% extension  │
└─────────────────────┘                      └─────────────────────┘
          │                                              │
          ▼                                              │
┌─────────────────────┐                                  │
│ EBSD tests for further│                                │
│ investigation        │                                 │
└─────────────────────┘                                  │
                                                         ▼
                                          ┌──────────────────────┐
                          ┌───────────────│ Waviness profiles for │
                          │               │ further investigation │
                          │               └──────────────────────┘
                          │                          ▲
                          ▼                          │
┌─────────────────────┐        ┌─────────────────────┐
│ Measurement using a 3D│──────▶│ Roughness profiles  │
│ laser scanning microscope│    └─────────────────────┘
└─────────────────────┘
```

more LABs were formed during recrystallisation with increasing annealing temperature and soaking time. This means that the LABs gradually develop into HABs during recrystallisation, which can be attributed to grain fragmentation caused by increasing strain [9]. The distributions of the CSL boundaries are depicted in Fig. 7(b) and the $\sum 3$ boundary is found to be dominant in the CSL boundaries. In general, the $\sum 3$ boundaries show lower mobility whilst the $\sum 5$, $\sum 7$ and $\sum 9$ boundaries are known to have high mobility [22]. The total fraction of the CSL boundaries shows a remarkable increase as the specimens are annealed under increasing temperature and soaking time. In addition, a noticeable increase in the

Fig. 4 The inverse pole figure (IPF) maps of the cold-rolled and annealed FSS sheet processed under (a) schedule A, (b) schedule B, (c) schedule C and (d) schedule D

(a)

(b)

(c)

(d)
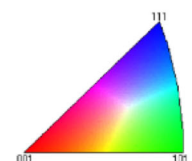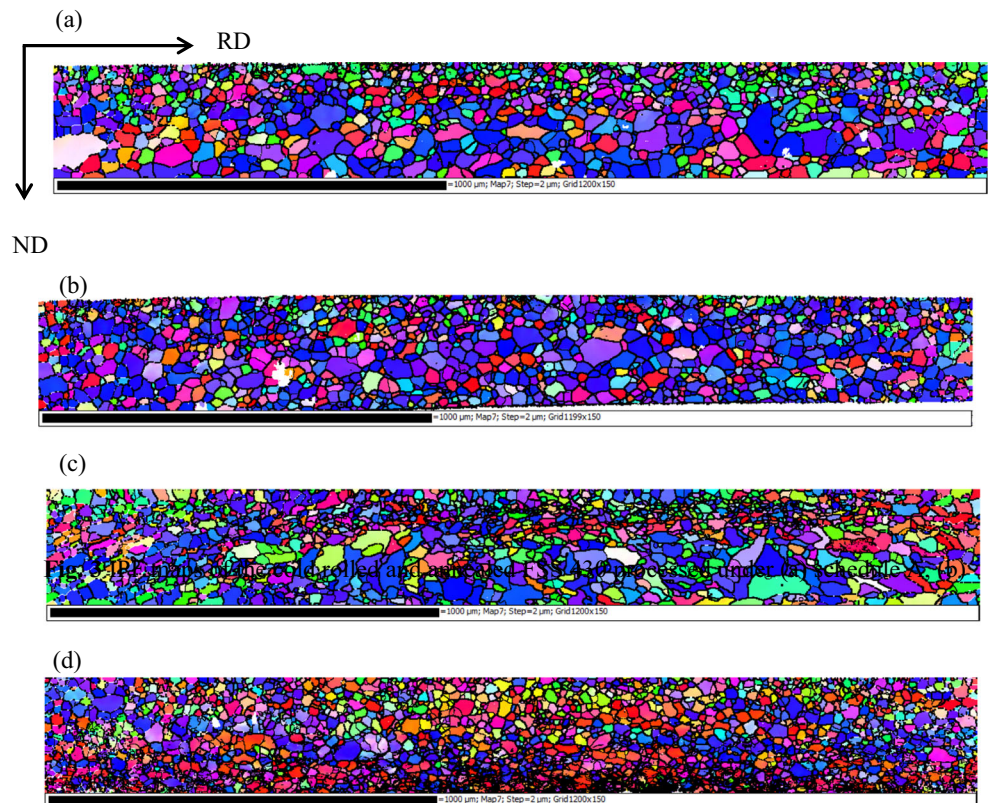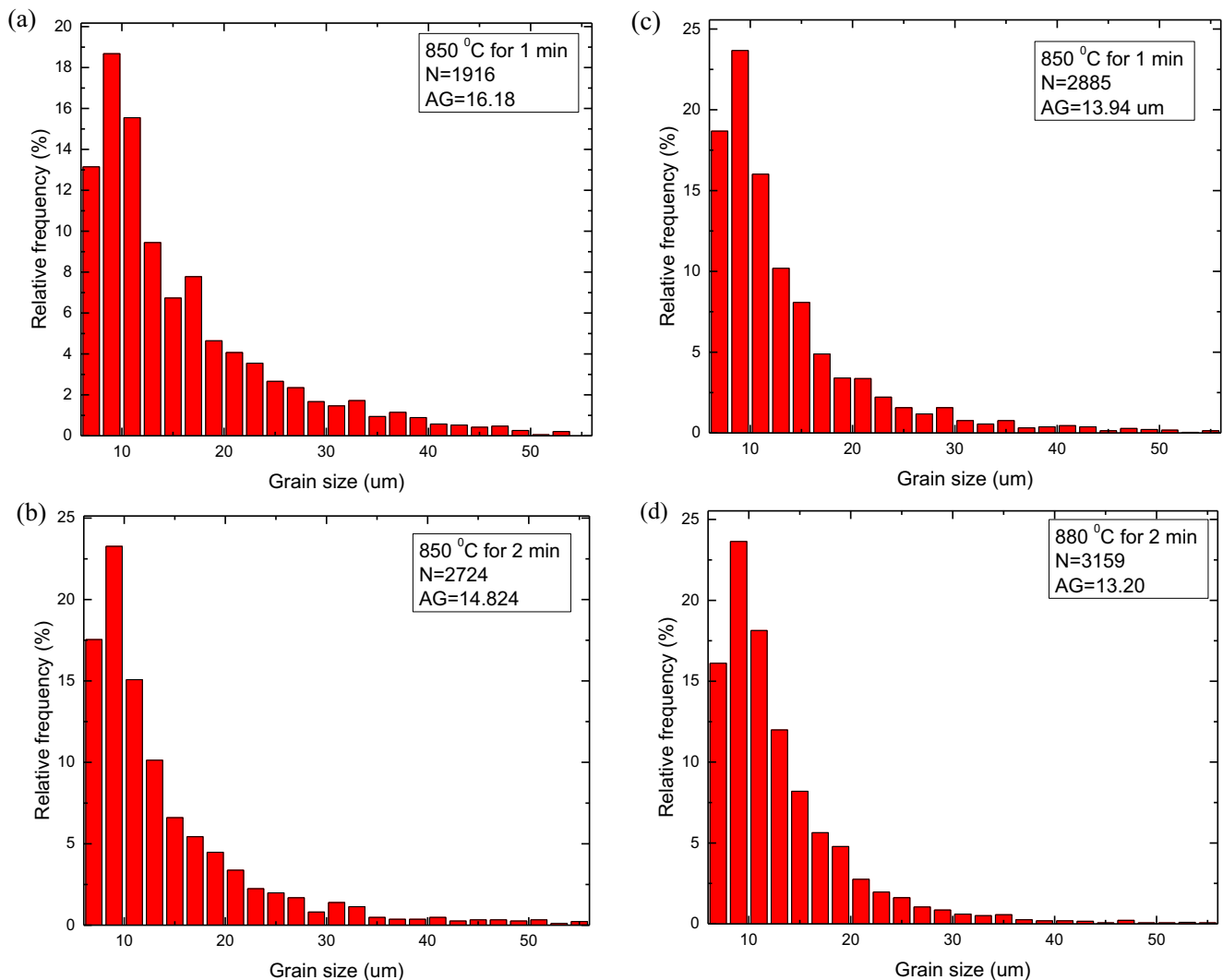
Fig. 5 Grain size distribution of the cold-rolled and annealed FSS 430 sheet processed under different schedules **a** schedule A, **b** schedule B, **c** schedule C and **d** schedule D

fraction of $\sum 3$ boundaries is observed with higher annealing temperature and soaking time, whilst the variation of the fraction of high-mobility boundaries is small.
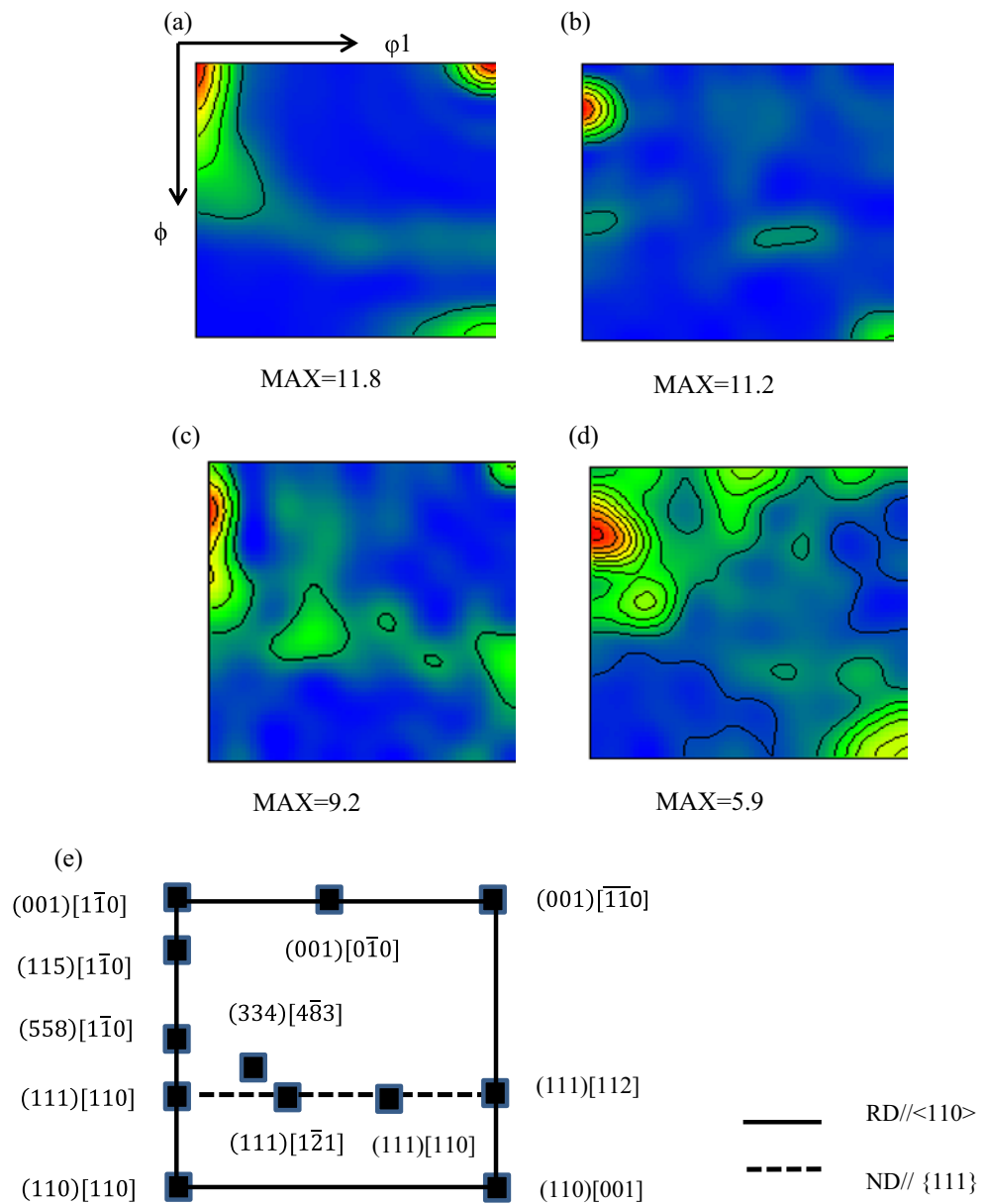
3 Discussion

3.1 The effect of annealing and the resultant microstructure and texture on ridging behaviour

The effects of annealing and the resultant microstructure and texture on the ridging severity of FSS during the forming processes are discussed in this section. It is commonly acknowledged that ridging is attributed mainly to the different plastic deformation of neighbouring grains with different crystal orientations after tensile deformation [23–27]. During the rolling processes, the grains at the surface layer suffer from shear strain whilst the grains at the central layers are deformed

due to plane strain. Pronounced texture gradients, such as the {001} <110> and {115} <110> components, are formed at central layers along with the formation of coarse bands whilst refined bands are formed at surface layers. After rolling processes, pancake-shaped grains survive and promote the formation of coarse grain bands in FSS 430. Given that the coarse bands with pronounced {115} <110> components are considered to be responsible for the ridging generation of FSS 430 after tensile deformation, a typical recrystallised texture with less pronounced gradients is recommended to enhance the ridging resistance of FSS 430.

To further investigate the correlation between annealing schedules, recrystallised grains and ridging severity, the recrystallisation fraction is calculated from the grain orientation spread (GOS) maps of FSS annealed under different schedules. The GOS maps show average misorientation angle between an average orientation of the grain and each orientation of scanned point. The microstructure of specimens can be

Fig. 6 ODFs ($\varphi2 = 45°$) of the cold-rolled and annealed FSS 430 processed under (a) schedule A, (b) schedule B, (c) schedule C and (d) schedule D, and (e) location of ideal orientations and fibres.

(a)

$\varphi1$

ϕ

MAX=11.8

(b)

MAX=11.2

(c)

MAX=9.2

(d)

MAX=5.9

(e)

$(001)[1\bar{1}0]$

$(115)[1\bar{1}0]$

$(558)[1\bar{1}0]$

$(111)[110]$

$(110)[110]$

$(001)[0\bar{1}0]$

$(334)[4\bar{8}3]$

$(111)[1\bar{2}1]$ $(111)[110]$

$(001)[\bar{1}\bar{1}0]$

$(111)[112]$

$(110)[001]$

—— RD//<110>

- - - - ND// {111}

distinguished to deformed and recrystallised region by GOS value, which is defined to be 1° in the present study [12]. As shown in Fig. 8. Drastic changes in the recrystallised fractions can be observed with the increase of annealing temperature and holding time. For specimens annealed under schedule D, the recrystallised fraction exceeds 95% which indicates that the grains were almost fully recrystallised. As a consequence, a refined microstructure with a smaller average grain size was formed with few coarse bands and better homogeneity inside FSS.

To evaluate the effect of recrystallised grains on the ridging generation of FSS, the impact of coarse grain bands is analysed. After cold rolling, the specimens were dominated by pancake-shaped grains with prominent bands of the cube and α-fibre components. The coarse grain bands were present inside the microstructure of specimens annealed under schedules A, B and C (as shown in Fig. 4), whilst such coarse bands were absent in the specimen processed under schedule D. Along with the elimination of coarse bands in specimens during recrystallisation, a remarkable reduction in ridging height can be observed on specimens stretched along the RD with 20% extension.

It is known that the clustering of grains with different sizes leads to varying yielding during forming due to the Hall-Petch effect [28], and the plastic deformation of grains with different sizes and Taylor factors can be different. The growth of grain sizes, therefore, promotes the irregularity generated by rotation and slip of grains during forming processes. To further investigate the effect of the coarse band on the surface ridging of FSS 430, the correlation between the coarse bands, average
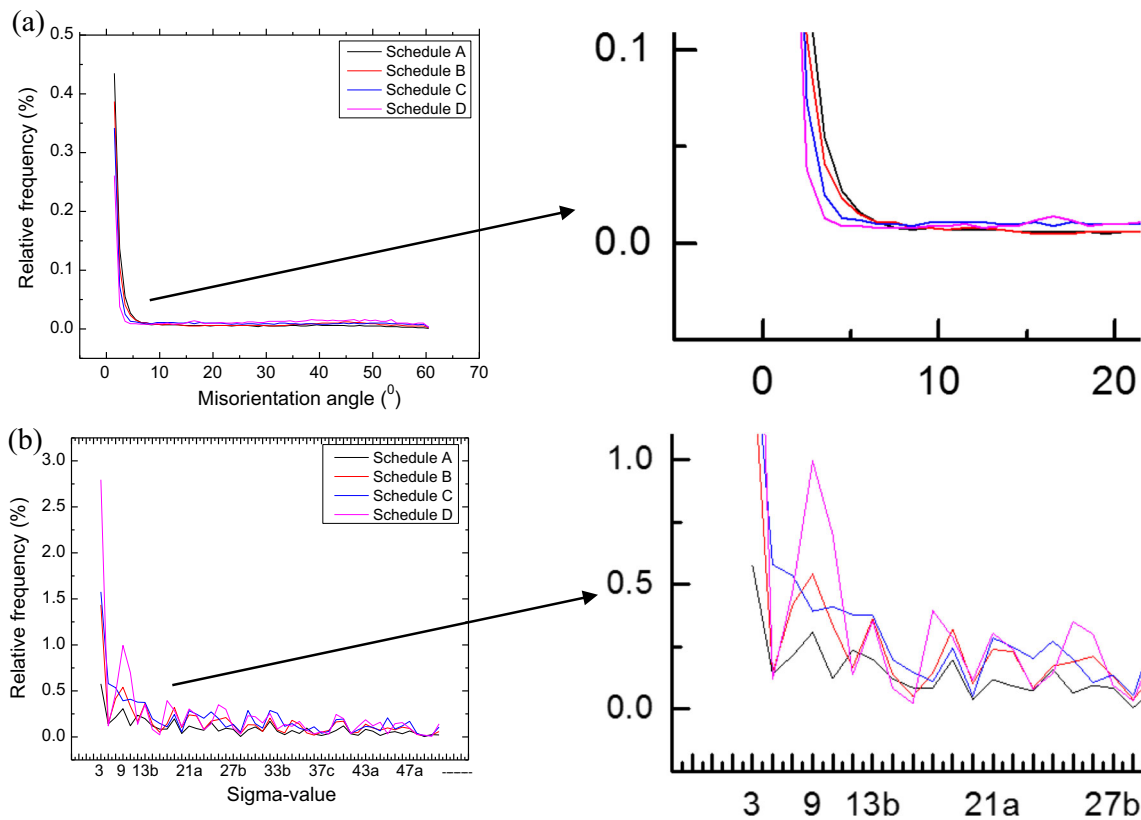
Fig. 7 (a) The distribution of the misorientation angle and (b) CSL boundary of FSS 430 annealed under different schedules

grain size and texture are analysed in the present study. Figure 9 shows the measured ridging height of FSS 430 with different average grain sizes. It can be seen from the curve that the ridging height is almost linearly dependent on the average grain size. It is known that the recrystallised grain size is dependent on the initial grain size before deformation and the strain incorporated within a grain during deformation [29, 30]. The coarse bands with cube orientation suffered less

rolling deformation and developed coarser ferrite grains after recrystallisation, inducing inhomogeneity of grain sizes at different layers of FSS 430. The remaining coarse bands, therefore, govern the average grain size and ridging height of FSS 430 during the forming processes.

Another impact of coarse bands on ridging generation of FSS is the texture. A comparison of the texture structure of refined grains and coarse grains was made in order to further investigate the correlation between grain bands and textures. The ODF sections were constructed by considering both refined grain bands and coarse grain bands of the cold-rolled and annealed specimens (as shown in Fig. 10 a). The coarse grain bands and refined grain bands are distinguished by the GOS values. It was found that the texture in both coarse grain bands and whole grain set were dominated by the {115} <110> component as indicated in Figs. 10 b and d, whilst the same in the refined grain set was dominated by a typical γ-fibre texture, Fig. 10 c. The results indicate that the impact of coarse grain bands on the texture of FSS can be dominant. The formation of coarse grain bands promotes the incomplete breakdown of crystals at different layers and the enhancement of the strength of the {115} <110> component, which promotes ridging generation on the surface of FSS 430 during the subsequent forming process [9].
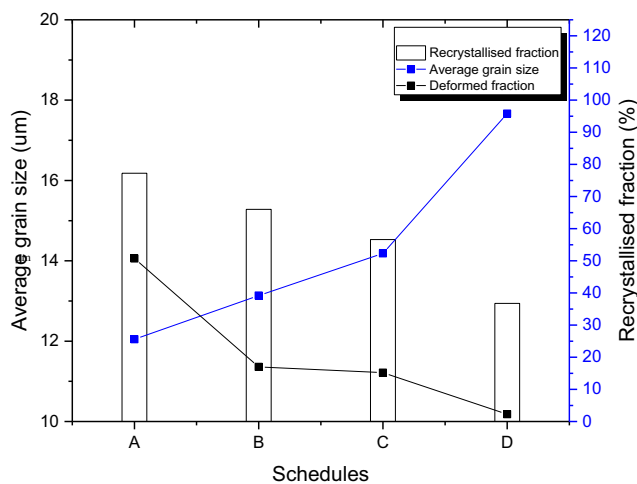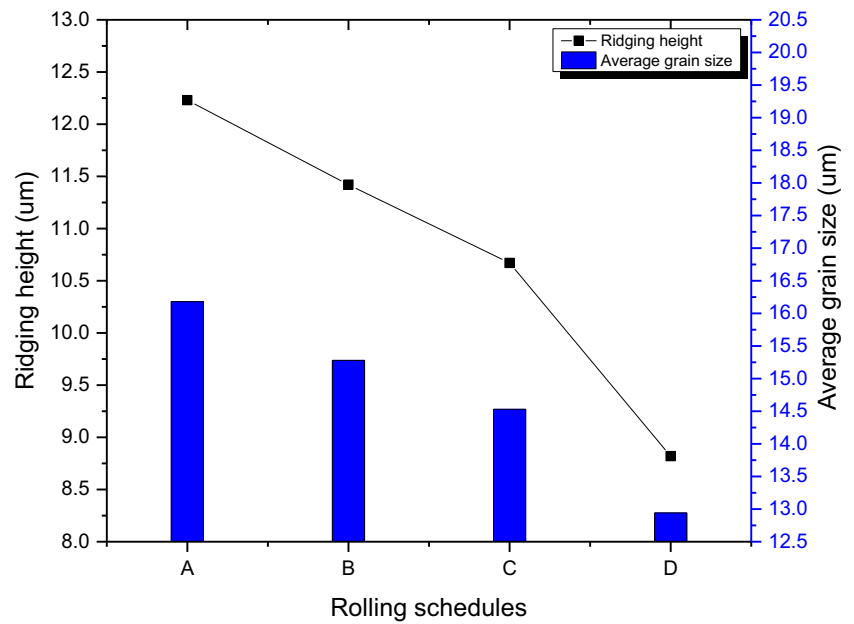
Figure 11 shows the orientation maps in specimens annealed under different schedules. Combined with Table 3

Fig. 8 Recrystallised fraction calculated from the GOS maps of specimens annealed under different schedules

Fig. 9 Ridging height of FSS 430 with different average grain sizes


which shows the fractions of different texture components, a slight decline of the {112} <110> component is observed with increasing annealing temperature and soaking time. This can be attributed to the refinement of the microstructure. It is known that the {112} <110> component is formed along with the generation of coarse bands at central layers [9]; the coarse grain bands were eliminated during recrystallisation and the {112} <110> components were, therefore, transformed into other components during annealing processes. For specimens annealed under schedule A, the fractions of the {111} <112> and {334} <483> components are found to be the lowest. With increasing annealing temperature and soaking time, remarkable increases in the {111} <112> and {334} <483> components are observed due to recrytallisation during annealing. In contrast, the fraction of the Goss orientation decreased when annealed under schedules C and D. In addition,

(a)

Refined grains

Coarse grains

(b)   (c)   (d)

MAX=21.6   MAX=6.4   MAX=11.2
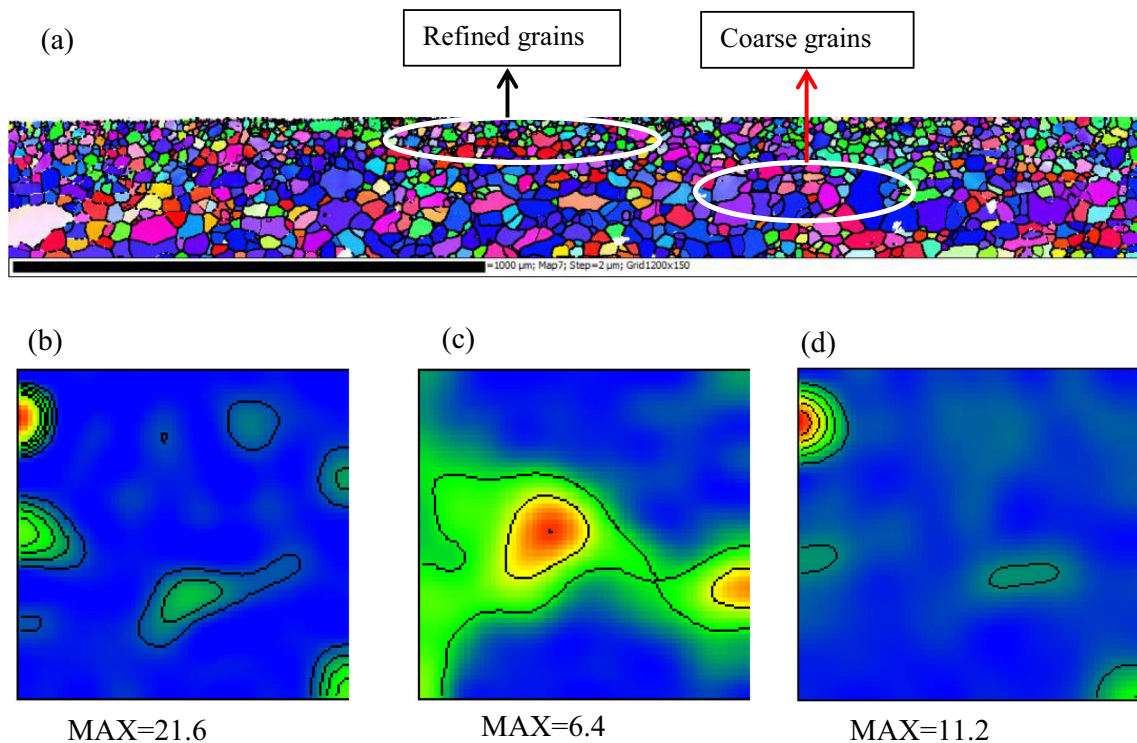
Fig. 10 $\phi 2 = 45°$ ODF sections of cold-rolled and annealed samples: **a** microstructure of the FSS 430 specimen annealed under schedule C, **b** coarse grains, **c** refined grains and **d** complete grain set
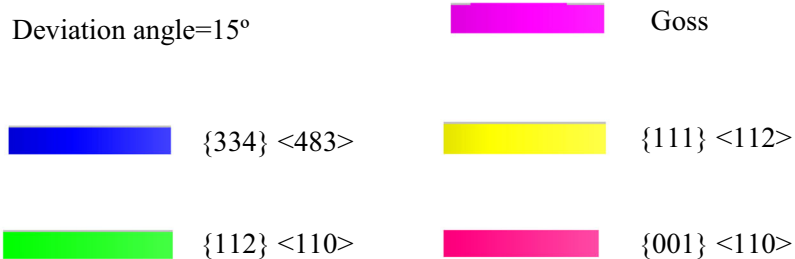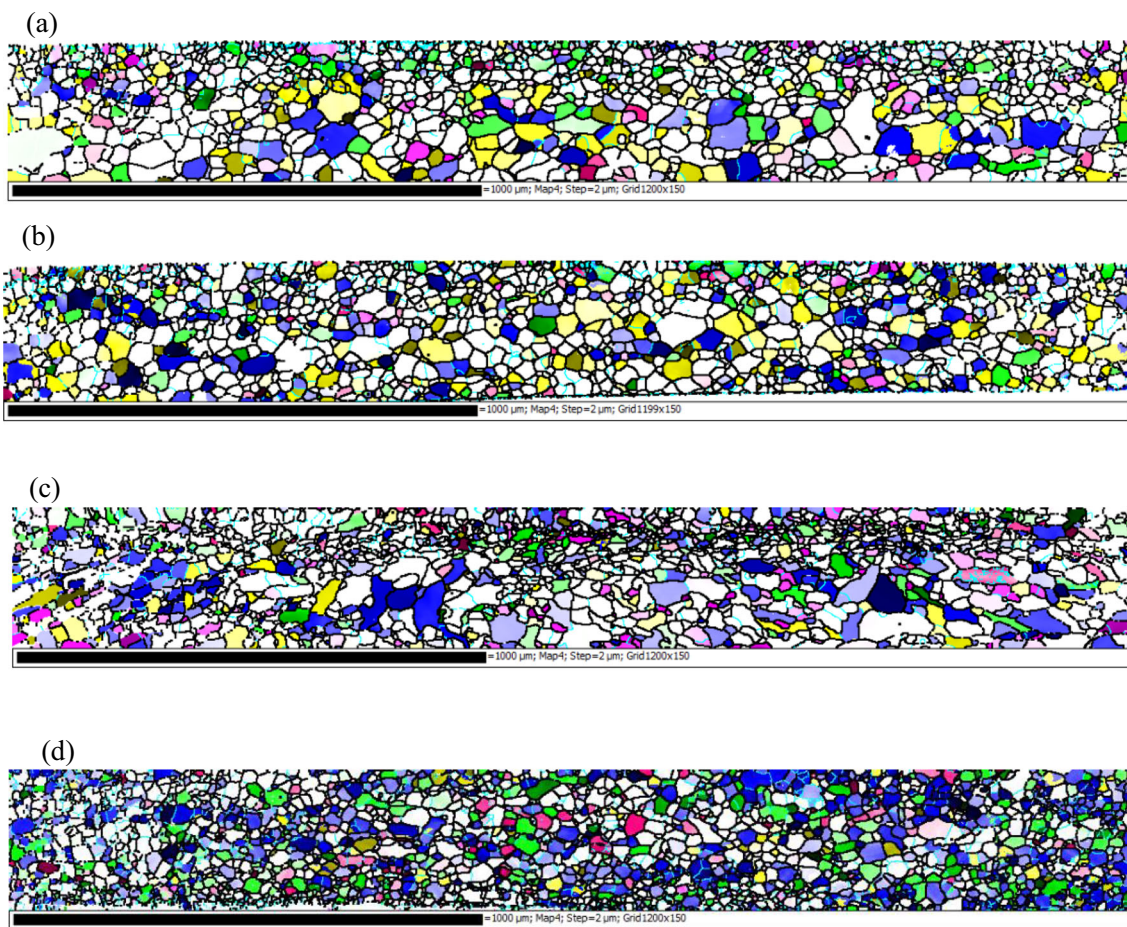
Fig. 11 Orientation maps of grains with 15° deviation from the ideal crystal orientation in specimens annealed under different schedules: (a) schedule A, (b) schedule B, (c) schedule C and (d) schedule D

Table 3 Fractions of major texture components in FSS 430 annealed under different schedules

Samples	Texture type				
	{001} <110>	{112} <110>	{111} <112>	{334} <483>	Goss
A	10.4	8.01	4.77	7.09	12.8
B	7.75	8.71	15.8	12.9	4.59
C	6.57	7.99	6.98	22.3	4.50
D	2.40	7.72	14.31	34.8	0.46

Fig. 12 3D surface topology of FSS 430 after 20% extension: **a** FSS annealed under schedule A, **b** FSS annealed under schedule B, **c** FSS annealed under schedule C and **d** FSS annealed under schedule D
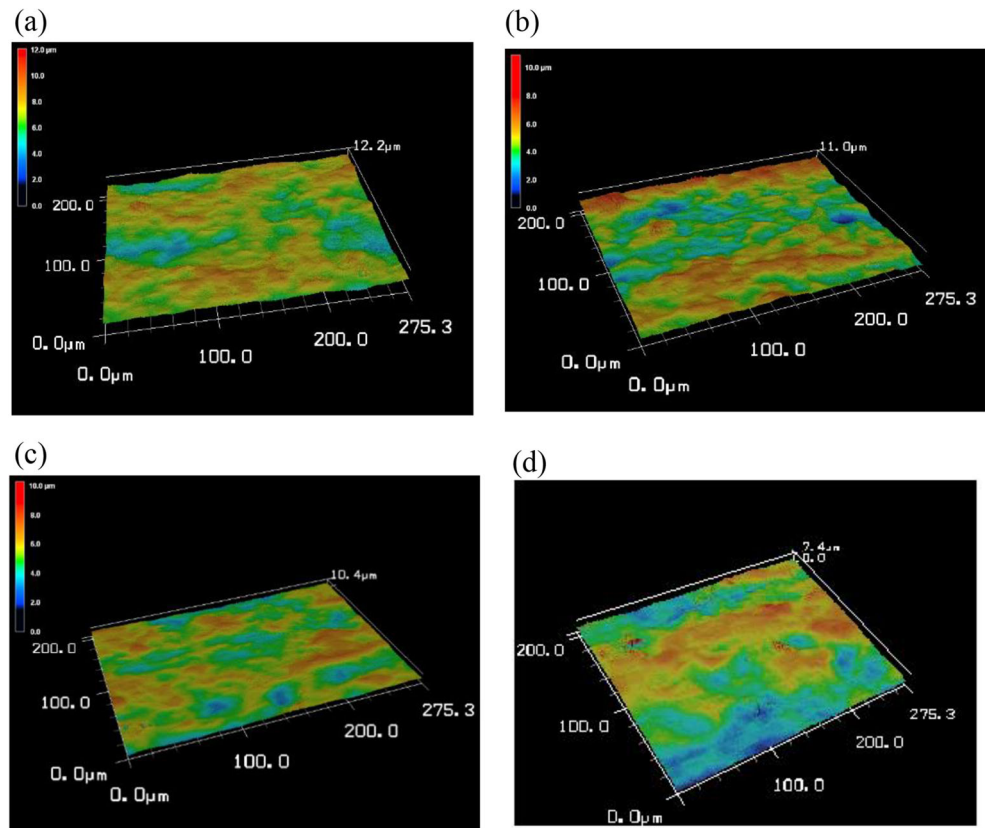
the rotation of Goss components into the {111} <112> component is presented during rolling processes [15], causing the formation of a typical BCC structure.

During the rolling processes, many coarse bands were formed with the {001} <001> component due to plane strain compression. During recrystallisation, the {001} <110> components transform into the {111} <112> component. The rate, however, is quite low due to the low stored energy. Many bands with the {001} <110> component, therefore, even survived after annealing processes and induced differential of plastic deformation with neighbouring grains, giving rise to the ridging height during the subsequent forming process. The {001} <110> component, therefore, is commonly considered to be the major component leading to ridging generation of FSSs [31]. The reduction in the {001} <110> components, therefore, is effective to improve the ridging severity of FSS during forming processes. A comparison of Figs. 10 and 11 reveals that the fraction of the {001} <110> component decreases along with the increase in the recrystallised fraction. During rolling processes, the {001} <110> component is formed along with the formation of coarse grain bands. This means that the reduction in the {001} <110> component indicates refinement in both the microstructure and the texture structure.

The recrystallisation during annealing promotes the microstructural refinement of FSS 430 and the formation of a typical BCC texture structure with less pronounced gradients, giving rise to the ridging resistance of FSS 430 during subsequent forming processes.

3.2 The effect of annealing and the resultant microstructure and texture on ridging behaviour

A quantitative assessment of the surface quality of the rolled sheets was utilised to reveal the ridging severity of specimens from sheets stretched by 20% parallel to the RD. Figure 12 shows the 3D surface topography of FSS 430 after tensile deformation on the specimens processed under different annealing schedules. It can be seen that the specimen annealed under schedule A shows a rough surface with significant undulations and ridges. The ridges are up to several centimetres in length and the maximum distance between peaks and gaps (ridging height) on the surface beyond 15 μm. In contrast, a smooth surface is observed on specimens annealed under schedule D. With increasing annealing temperature and holding time, the surface quality is found to be improved with lower ridging height and fewer undulations on the surface of FSS 430. For specimens with extended soaking time and increased annealing temperature, remarkable improvement can be observed on the ridging severity of FSS after tensile deformation and a maximum of 50% reduction in the ridging height can be achieved using optimised parameters during the

Fig. 13 Waviness profiles of FSS 430 along the TD after 20% extension: **a** FSS annealed under schedule A, **b** FSS annealed under schedule B, **c** FSS annealed under schedule C and **d** FSS annealed under schedule D
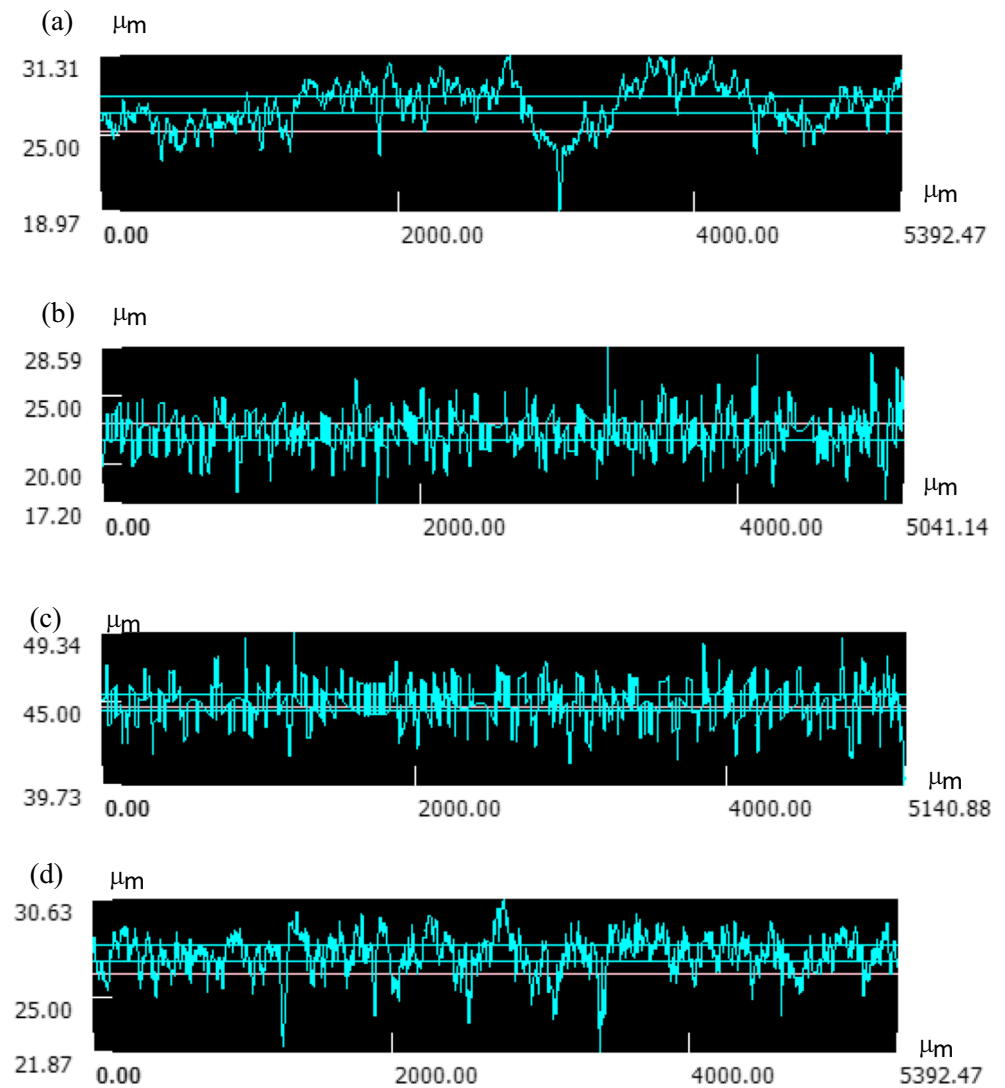
annealing process. This conclusion can be also supported by research from Park et al. [12]. It was found that the ridging height of FSS reduced by 50% with the soaking time increased from 30 s to 5 h.

Figure 13 shows the waviness profiles of specimens annealed under different schedules. The raw data reveal pronounced undulations on the surface of FSS 430 with shortwave noise and roughness. To eliminate noise and enhance the accuracy of the results, the raw data were transformed with a discrete Fourier transform so that the low-frequency parts were removed. A roughness profile, therefore, is created by removing the long-wavelength component from the primary profile and a waviness profile is created by removing the short-wavelength component from the primary profile. The ridging height is thereby calculated by measuring the maximum gap between peaks and valleys in the waviness profile. A comparison of the measured results between schedule A and D indicates that the ridging height decreased from 12.3 to 8.8 μm with increasing annealing temperature and soaking time. Table 4 shows the low ridging height of FSS achieved by the proposed rolling route compared with previous research. Therefore, the optimisation of rolling route by extending soaking time and increasing annealing temperature is considered to be effective to improve the ridging resistance of FSS during subsequent forming processes.

Table 4 Achieved ridging height of FSS 430 compared with previous research

Samples	In the present study	Shin et al. [26]	Park et al. [12]	Huh et al. [32]
Ridging height (μm)	10.4	19.8	16.6	12.7

4 Conclusions

Ridging is a 'surface defect' that is commonly encountered during the forming process of FSS. A systematic study was conducted in order to identify the effect of annealing schedules on the microstructure, texture and ridging severity of FSS 430 during subsequent forming processes. The major conclusions derived from the present study are listed below:

(1) During final annealing step, the specimens annealed under 880 °C for 3 min (schedule D) were found to exhibit the highest recrystallisation fraction of FSS 430, which contributes to the microstructural refinement and optimised texture structure. The ridging height was found to be reduced with increasing recrystallisation fraction due to the microstructural refinement, especially in central layers of FSS 430.

(2) The formation of coarse grain bands promotes the incomplete breakdown of crystals at different layers and the enhancement of the strength of specific texture components, which induces a raised ridging height on the surface of FSS 430 during the forming process.

(3) A remarkable reduction in the {001} <110> component was found along with increasing recrystallisation fraction. With low stored energy and Taylor factor, the {001} <110> component is considered to be one of the major causes of ridging generation. With high temperature and extended soaking time during annealing, the coarse bands with {112} <110> and {001} <110> components can be refined to overcome the ridging defect in FSS 430.

References

1. Chao HC (1967) The mechanism of ridging in ferritic stainless steels. Trans ASM 60(1):37–50
2. Takechi H, Kato H, Sunami T, Nakayama T (1967) The mechanism of ridging phenomenon in 17% chromium stainless steel sheets. Trans JIM 31(6):717–723
3. Engler O, Schafer C, Brinkman HJ (2012) Crystal-plasticity simulation of the correlation of microstructure and roping in AA 6xxx Al-Mg-Si sheet alloys for automotive applications. Acta Mater 60: 5217–5232
4. Knutsen R, Wittridge N (2002) Modelling surface ridging in ferritic stainless steel. Mater Sci Technol 18:1279–1285
5. Huh M, Engler O (2001) Effect of intermediate annealing on texture, formability and ridging of 17% Cr ferritic stainless steel sheet. Mater Sci Eng A 308:74–87
6. Bennett T, Petrov R, Kesten L (2009) Texture-induced surface roping in an automotive aluminium sheet. Scr Mater 61:733–736
7. Baczynski G, Guzzo R, Ball M, Lloyd D (2000) Development of roping in an aluminium automotive alloy AA6111. Acta Mater 48: 3361–3376
8. Patra S, Singhal L (2013) Influence of hot band annealing and cold rolling on texture and ridging of 430 stainless steel containing aluminum. Mater Sci Appl 4:70–76
9. Patra S, Ghosh A, Sood J, Singhal LK, Podder AS, Chakrabarti D (2016) Effect of coarse grain band on the ridging severity of 409L ferritic stainless steel. Mater Des 106:336–348
10. Zhang C, Liu Z, Wang G (2011) Effects of hot rolled shear bands on formability and surface ridging of an ultra purified 21%Cr ferritic stainless steel. J Mater Process Technol 211:1051–1059
11. Gao F, Yu F, Misra R, Zhang X, Zhang S, Liu Z (2015) Microstructure, texture, and deep drawability under two different cold-rolling processes in ferritic stainless steel. J Mater Eng Perform 24:3862–3880
12. Park J, Park S (2012) Effect of heat treatment on a ridging phenomenon of ferritic stainless steels. Metal
13. Han J, Li H, Zhu Z, Jiang L, Xu H, Ma L (2014) Effects of processing optimisation on microstructure, texture, grain boundary and mechanical properties of Fe-17Cr ferritic stainless steel thick plates. Mater Sci Eng A 616:20–28
14. Mola J, Jung I, Park J, Chae D, Cooman B Ridging control in transformable ferritic stainless steels. Metall Mater Trans A 43: 228–244
15. Dorner D, Zaefferer S, Raabe D (2007) Retention of the Goss orientation between microbands during cold rolling of an Fe3%Si single crystal. Acta Mater 55(7):2519–2530
16. Zaefferer S, Baudin T, Penelle R (2001) A study of the formation mechanisms of the cube recrystallization texture in cold rolled Fe-36%Ni alloys. Acta Mater 49(6):1105–1122
17. ASTM Standard E8-E8M -08 (2008) Standard test methods for tension testing of metallic materials. ASTM International, West Conshohocken
18. Kang SG, Kobayashi T (2004) Asymmetric rolling as means of texture and ridging control and grain refinement of aluminum alloy and steel sheets. Mater Sci Forum 449:1–6
19. Ma XG, Zhao JW, Du W, Zhang X, Jiang ZY (2017) An analysis of ridging of ferritic stainless steel 430. Mater Sci Eng A 685(8):358–366
20. Ma X, Zhao J, Du W, Zhang X, Jiang Z (2018) Effect of rolling processes on ridging generation of ferritic stainless steel. Mater Charact 137:201–211
21. Siqueira R, Sandim H, Oliveira T, Raabe D Composition and orientation effects on the final recrystallisation texture of coarse-grained Nb-containing AISI 430 ferritic stainless steels. Mater Sci Eng A 528:3513–3519
22. Hawakaya Y, Szpunar J, Paulambo G, Lin P (1996) The role of grain boundary character distribution in goss texture development of electrical steel. J Magn Magn Mater 160:143–144
23. Lefebvre G, Sinclair CW, Lebensohn R, Mithieux JD (2012) Model Simul Mater Sci Eng 20:1–16
24. Jung I, Mola J, Chae D, Coonan BC (2010) Influence of the cold rolling and annealing sequence on the ridging behaviour of Ti-stabilized 18% Cr ferritic stainless steel. Int J Steel Res 81(12): 1089–1096
25. Howell P, Fleet D, Welch P, Ralph B (1978) Texture and grain boundary structure in tungsten-III. The primary misorientation function and grain boundary structure. Acta Metall 26:1499–1503

26. Raabe D, Sachtleber M, Weiland H, Scheele G, Zhao Z (2003) Grain-scale micromechanics of polycrystal surfaces during plastic straining. Acta Mater 51(6):1539–1560

27. Park S, Kim K, Lee Y, Park C (2002) Evolution of microstructure and texture associated with ridging in ferritic stainless steels. ISIJ Int 42:100–105

28. Shin HJ, An JK, Park SH, Lee DN (2003) The effect of texture on ridging of ferritic stainless steel. Acta Mater 51:4693–4706

29. Sellars C, Whitema J (1979) Recrystallisation and grain growth in hot rolling. Met Sci 13:187–194

30. Wright RN (1972) Anisotropic plastic flow in ferritic stainless steels and the roping phenomenon. Metall Trans 3(1):83–91

31. Viana C, Pinto A, Candido F, Matheus R (2006) Analysis of ridging in three ferritic stainless steel sheets. Mater Sci Technol 22:293–300

32. Huh M, Lee J, Park S, Engler O, Raabe D (2005) Effect of through-thickness macro and micro-texture gradients on ridging of 17%Cr ferritic stainless steel sheet. Steel Res Int 76(11):797–806